A New Method for Coverage Prediction for the Wide Area Augmentation System (WAAS)

Samuel P. Pullen, Per K. Enge, and Bradford W. Parkinson

Department of Aeronautics and Astronautics
Stanford University

BIOGRAPHIES

Sam Pullen is a Ph.D. student and research assistant in the Gravity Probe-B project at Stanford University. An S.B. Graduate of MIT, he conducts research on spacecraft design for reliability and robust control design along with studies of GPS augmentation system performance and integrity.

Per Enge is a Research Professor of Aeronautics and Astronautics at Stanford University. A Ph.D. graduate of the University of Illinois, his research focuses on WAAS aircraft landing applications. He previously taught at WPI and is the ION Satellite Division Chairman.

Brad Parkinson is a Professor of Aeronautics and Astronautics at Stanford University and is the program manager for the Gravity Probe-B relativity gyro experiment. He served as the first Program Director of the GPS Joint Program Office and was instrumental in the system's development.

ABSTRACT

To provide a detailed analysis framework for WAAS accuracy prediction, a new method has been developed which combines GPS geometry simulation with least-squares covariance analysis. This approach considers all standard ranging errors for each WAAS reference station receiver and user, including satellite clock, SA-induced latency, ephemeris, multipath, receiver noise, troposphere and ionosphere errors. Computer simulation allows us to project mean, 2σ, and 3σ position error for a grid of user positions across a wide geographic area.

The simulation updates orbit positions of the GPS satellites augmented by four geosynchronous spacecraft. For each resulting geometry, satellite geometry for all WRS's is determined. The simulation then loops through a grid of user positions. The satellite geometry for each user is computed, and the user's clock/ephemeris error is projected through covariance matrices that link the error at each WRS to the user (including non-WAAS errors).

Ionosphere errors are handled by a separate covariance algorithm running in parallel. This algorithm uses a MITRE-like grid of ionosphere corrections, but instead of using interpolation, a "truth" model of vertical ionosphere covariances is developed and projected (using a weighted least-squares solution) from the WRS pierce points to the master station grid. The user then projects the error covariances back to his own pierce points (including non-iono. WRS errors). The resulting clock/ephemeris and ionosphere covariances for each user are added together. The user then computes a weighted least-squares position and finds his expected 1σ position error from the resulting covariance.

The simulation stores histograms of vertical position error at each grid point and compares them to the 4.1-m 2σ ILS navigation requirement for airborne Category I precision landing. Availability is tabulated for each user position, as is the maximum availability outage period. Results presented for the Stanford 3-WRS experimental WAAS network show that the Stanford WAAS meets this accuracy requirement over a large area. The results also validate the observed vertical errors from Stanford's WAAS flight trials. Finally, this paper presents accuracy coverage predictions for proposed FAA NSTB WAAS testbed networks that cover the entire Continental U.S.

1.0 Introduction

To date, studies of corrected pseudorange accuracy and satellite availability for prototypes of the Wide Area Augmentation System (WAAS) have demonstrated the potential to achieve vertical position accuracies of 2-3 meters at specific user sites [1]. Experiments conducted to date at sites far from the nearest reference station seem to confirm this [2]. However, it remains unclear how results achieved at specified user locations can be extended to predict user accuracies across a wide geographic area, which is the purpose of WAAS. Therefore, while it is apparent that WAAS has the potential to provide Category I accuracy for aircraft landing and that baselines of hundreds of kilometers are possible, it is not clear just how many wide-area

reference stations (WRS's) are needed to meet accuracy requirements over the entire geographic spread of users.

The development of WAAS is taking place in stages. Small networks of 3 or 4 WRS's have been built by Stanford and others to do preliminary tests. The FAA plans to build a WAAS testbed (known as NSTB) prior to development of a 29-WRS's operational WAAS [3]. Studies to date have used the layout of these preliminary networks to examine the geographic separation between users and WRS's and between ionospheric *pierce points*; i.e., the points at which the line-of-sight from GPS satellite to user pierces the ionosphere [7]. Their results suggest designing networks of WRS's that are both numerous enough and in close-enough proximity to ensure that users are "close enough" to the nearest WRS with near-certainty. WAAS networks are currently laid out with the help of only these preliminary guidelines.

This paper presents a method for expanding on our current understanding of WAAS performance capability by projecting linear least-squares error *covariance* matrices from WRS's through the master station (WMS) to users. Although this approach abstracts the detailed workings of the WRS's and WMS, it succeeds in modeling the underlying error uncertainties; thus the results are indicative of the performance that can be achieved by a canonical WAAS architecture. It allows user accuracy predictions over a wide geographic area for any proposed network of WRS's and geosynchronous satellites (which communicate WAAS corrections and serve as redundant ranging sources).

This paper describes this new "coverage prediction" methodology in detail, including the ranging error variances and least-squares covariance equations. Results are then displayed for the Stanford network of 3 WRS's in California and Nevada, along with variations which examine the effects of adding a WRS in Hawaii. Results for a much larger network, the proposed FAA WAAS testbed (NSTB), are then shown, along with studies of variations of the baseline NSTB network. The results demonstrate the utility of WAAS accuracy predictions over large areas, and they point out possible weaknesses in the coverage provided by the WAAS networks mentioned above. This allows sensitivity studies to be conducted that promise to greatly aid the process of designing future wide-area systems.

2.0 Overview of WAAS Simulation Approach

The coverage prediction approach used here is based on the solution of least-squares covariance equations for given GPS and WRS geometries. Accuracy predictions for large geographic areas are generated by a computer program which simulates a large number N_t (between 1440 and 10,000) of separate GPS and geosynchronous satellite geometries using a GPS orbit model. The orbit model uses the Volpe almanac data for the 24 GPS satellites and includes three geosynchronous satellites located over the Equator at longitudes 180°, 63° E, and 55° W respectively. The first and third of these can be seen by users in the Continental U.S. Spacecraft are assumed to always be working (i.e. no failure sampling), and geometries are sampled in either of two ways: (1) random time updates sampled from a Uniform[0, 30 min] distribution, and (2) constant 1-minute time updates. In case (2), one day (1440 trials) of satellite orbits is cycled through, and it is possible to keep track of the *maximum outage duration* at each user site, which is the longest period in which predicted vertical position accuracy does not meet the 4.1-m ILS Category I requirement. This ILS requirement is considered ambitious for WAAS; thus a more-flexible RNP Tunnel requirement of 6 to 7.6 m is under consideration and can also be examined here [9].

For each satellite geometry, the matrix of direction cosines to each visible satellite $\mathbf{G}_w^i$ is computed for each WRS location *i* (using a 5° mask angle). At this stage, the ranging observation errors for each satellite visible at each WRS are computed from the RMTSA model in Section 3.0, and the large WRS ionosphere covariance matrix $\mathbf{P}^P$ can be computed element-by-element. The program then cycles through a grid of user locations separated by 1-3 degrees in latitude and longitude. For each user, the geometry matrix $\mathbf{G}_u$ is computed, and two separate processes of covariance propagation are carried out in parallel. The first is the *clock/ephemeris* error for satellites in view of the user (using a 7.5° mask angle) based on the WRS's that can see that satellite and can thus provide clock/ephemeris corrections. The second is *ionospheric* spatial decorrelation projected from the pierce points observed by each WRS to the WMS, which fits a set of predictions to a grid, and finally to each user.

Covariance projections from ionosphere and RMTSA error sources are brought together into a single pseudorange error covariance matrix $\mathbf{P}_v^*$ for each user. Using the matrix $\mathbf{P}^{SV}$ of clock/ephemeris errors for each satellite, the weighted least-squares position error covariance $\hat{\mathbf{P}}_x$ is computed, and the vertical position error variance (assumed to be Gaussian) is given by the [3,3] entry of this final matrix. The vertical error result for each geometry is stored in a histogram for that user, as is the Vertical DOP for the satellite geometry visible to that user [10]. "Availability" in this case is defined as the percentage of geometries for which a given user's vertical one-sigma error (given by $\sqrt{\hat{\mathbf{P}}_x[3,3]}$) is within

the ILS one-sigma requirement of 2.05 meters. Geometries for which this requirement is exceeded are deemed "non-available", and if this state persists over time, an "outage period" for Category I landings results.

Figure 1 gives a conceptual flow chart for this covariance propagation method. Sections 4.0 and 5.0 describe the algorithms for computing clock/ephemeris and ionosphere covariances, and Section 3.0 gives the receiver-specific RMTSA ranging error model used. The relevant equation numbers are referenced in the figure.

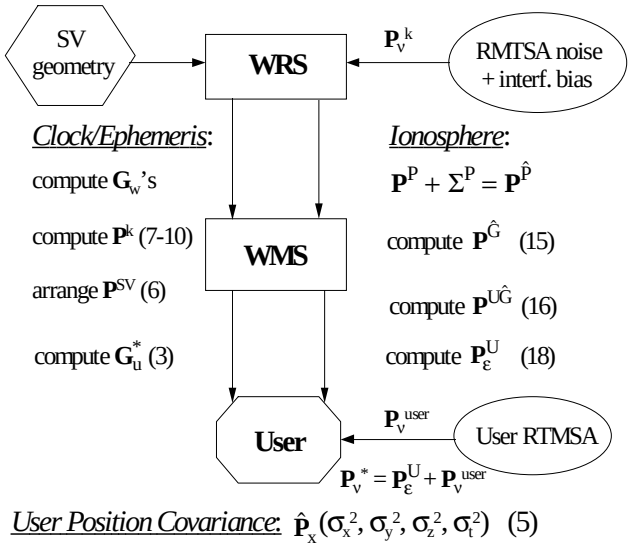

Figure 1: WAAS Covariance Overview

3.0 RMTSA Ranging Error Model

WAAS employs GPS corrections computed by a network of reference stations to remove most of the satellite-based errors that exist without differential corrections. This process is modeled by the propagation of clock/ephemeris and ionosphere covariances described here. However, it is corrupted by receiver and location-specific errors at each WRS and at the user. These errors are collectively labeled RMTSA, representing receiver noise, multipath, troposphere, and remaining Selective Availability errors. In this analysis, these errors are assumed to be independent and Normally distributed; thus their combined variance can be obtained by taking the sum of the individual noise variances.

Noise Source	WRS Error (m)	User Error (m)
receiver noise	0.33	0.50
SA latency	not applicable	0.20
multipath	$0.20 / \tan(\varepsilon)$	$0.30 / \tan(\varepsilon)$
troposphere	$0.176 / \sin(\varepsilon)$	$0.176 / \sin(\varepsilon)$

Table 1: One-Sigma RMTSA Errors

Table 1 gives the individual error standard deviations for each individual RMTSA error source. With the exception of troposphere, WRS errors are assumed to be of smaller magnitude compared to a generic single-frequency user receiver. User SA latency error assumes a fast-correction average age of 10 seconds [13]. Note that both multipath and troposphere errors are functions of the elevation angle ε from the user to the satellite in question. This represents the additional "slant" delay due to atmospheric effects and the greater GPS signal reflection magnitude for lower satellite elevations. RMTSA error terms are introduced into the covariance equations as diagonal *n* x *n* matrices (where *n* satellites are in view) in which each diagonal element contains the combined RMTSA variance for that satellite.

The error sizes in Table 1 are not meant to be especially conservative. Instead, they represent a reasonable estimation of the errors that will be experienced by WAAS-certifiable equipment. More conservative noise distributions have been used in other studies [8] to show the position accuracy degradation that might result from "looser" hardware standards.

4.0 Clock/Ephemeris Covariance Prediction

4.1 Covariance Prediction Equations

The covariance model developed here separates clock/ephemeris errors from all other ranging error sources. Thus, both ionosphere errors (Section 5.0) and RMTSA errors (Section 3.0) appear as external error inputs to the clock/ephemeris prediction equations. In this approach, user pseudorange error $\Delta\rho$ is expressed as a combination of ephemeris (Δr), clock error (Δb), and other terms (after corrections are applied) as follows:

$$\Delta\rho = \mathbf{G}_u \begin{bmatrix} \Delta r_u \\ \Delta b_u \end{bmatrix} - \tilde{\mathbf{G}}_u \Delta x^{SV} + \nu_u \qquad (1)$$

where $\mathbf{G}_u$ is the user direction-cosine satellite geometry matrix (size K x 4, where K is the number of satellites in view) and ν is a term representing a Gaussian white-noise model of other error sources. The augmented matrix $\tilde{\mathbf{G}}_u$ of size K x 4K is constructed by placing each row of $\mathbf{G}_u$ along a diagonal pattern as follows:

$$\tilde{\mathbf{G}}_u = \begin{bmatrix} -1_u^{k_1} & 1 & 0 & 0 & \cdots & 0 & 0 \\ 0 & 0 & -1_u^{k_2} & 1 & \cdots & 0 & 0 \\ \vdots & \vdots & \vdots & \vdots & \vdots & \vdots & \vdots \\ 0 & 0 & 0 & 0 & \cdots & -1_u^{K} & 1 \end{bmatrix} \qquad (2)$$

Since (1) conceptually includes all GPS error sources, we can proceed to find position error covariance from it.

The standard pseudoinverse definition for an overdetermined system (more satellites in view than unknowns) is:

$$\mathbf{G}_u^* = \left(\mathbf{G}_u^T \mathbf{G}_u\right)^{-1} \mathbf{G}_u^T \tag{3}$$

Here, we find the user position fix error by weighted least squares, where the weighting matrix **W** is given by the user pseudorange error matrix $\mathbf{P}_\nu$ to be defined next:

$$\hat{x}_u = \mathbf{G}_u^{wt*} \Delta\rho = \left(\mathbf{G}_u^T \mathbf{W}^{-1} \mathbf{G}_u\right)^{-1} \mathbf{G}_u^T \mathbf{W}^{-1} \Delta\rho \tag{4}$$

Using the definition of covariance, the final user position error covariance $\mathbf{P}_{\hat{x}}$ is given by:

$$\mathbf{P}_{\hat{x}} = \mathbf{G}_u^* \tilde{\mathbf{G}}_u \mathbf{P}^{SV} \tilde{\mathbf{G}}_u^T \left(\mathbf{G}_u^*\right)^T + \mathbf{G}_u^* \mathbf{P}_\nu^* \left(\mathbf{G}_u^*\right)^T \tag{5}$$

where $\mathbf{P}_\nu^*$ is the K x K diagonal matrix of user noise variances for each satellite due to ionosphere and RMTSA errors. It is calculated from the combined results of the ionosphere covariance model (Section 5.0) and the RMTSA model (Section 3.0). The use of this matrix as **W** in (4) above should give a minimum-variance estimate of the true user position, but in this model, we assume that **W** cannot be known perfectly by the user. Instead, each entry of **W** is calculated by sampling from a Normal distribution whose mean is the corresponding entry of $\mathbf{P}_\nu$ and whose standard deviation is a fixed ratio of that mean (usually 25%). We have found that the WAAS accuracy results are not very sensitive to this "uncertainty ratio" if it is below 75%.

$\mathbf{P}^{SV}$ in (5) is a user-specific block diagonal matrix of K separate 4 x 4 covariance matrices as follows:

$$\mathbf{P}^{SV} = \begin{bmatrix} \mathbf{P}^{k_1} & 0 & 0 \\ 0 & \ddots & 0 \\ 0 & 0 & \mathbf{P}^K \end{bmatrix} \tag{6}$$

These separate covariance matrices $\mathbf{P}^{k_1}$, ..., $\mathbf{P}^K$ each represent the post-correction covariance in *x*, *y*, and *z* components of spacecraft ephemeris, as well as the clock error in *t*. If no WAAS corrections are available (because this satellite is not visible to any WRS), this matrix has diagonal terms representing uncorrected C/A code noise variances as follows [14]:

$$\mathbf{P}_{no}^k = \begin{bmatrix} \frac{|\Delta r_k|^2}{3} & 0 & 0 & 0 \\ 0 & \frac{|\Delta r_k|^2}{3} & 0 & 0 \\ 0 & 0 & \frac{|\Delta r_k|^2}{3} & 0 \\ 0 & 0 & 0 & \frac{|\Delta B_k|^2}{3} \end{bmatrix} = \begin{bmatrix} 9 & 0 & 0 & 0 \\ 0 & 9 & 0 & 0 \\ 0 & 0 & 9 & 0 \\ 0 & 0 & 0 & 100 \end{bmatrix} (m^2) \tag{7}$$

If WAAS corrections are available from at least one WRS (assume M > 0 WRS's can see a given satellite), we form the matrix $\mathbf{G}_w$ as follows for each satellite *k*, where *k* = 1,2,...,K:

$$\mathbf{G}_w = \begin{bmatrix} \mathbf{1}_{m_1}^k & -1 \\ \mathbf{1}_{m_2}^k & -1 \\ \vdots & \vdots \\ \mathbf{1}_M^k & -1 \end{bmatrix} \tag{8}$$

where $\mathbf{1}_m^k$ is the direction-cosine vector from WRS *m* to satellite *k*. Note that the clock/ephemeris error can be estimated directly by weighted least squares. However, a direct solution (such as in equation (4)) tends to be too sensitive to measurement errors for underdetermined and exactly-determined (M = 4) cases. Instead, we include a a prior state covariance matrix Λ and solve the problem as a Kalman-filtered measurement update to the prior covariance. The inclusion of prior information helps ensure that a wildly unlikely solution is not force-fit by "naive" least squares [14].

Although normally the matrix Λ would be the same as the prior (no corrections) covariance in (7), we have the freedom to vary the diagonal-entry "weights" of the matrix. We do this by multiplying the *x*, *y*, and *z* variances by a factor of 10, which effectively increases the weight we assign to the WRS measurements. Further, we make the prior clock variance very large since it will in reality be estimated separately from ephemeris, and we wish to avoid the prior clock variance from affecting the ephemeris estimates much. Our final choice for the state prior covariance is:

$$\Lambda = \begin{bmatrix} 90 & 0 & 0 & 0 \\ 0 & 90 & 0 & 0 \\ 0 & 0 & 90 & 0 \\ 0 & 0 & 0 & 1\times10^{6} \end{bmatrix} \quad (m^2) \qquad (9)$$

The measurement-update equation for the WAAS-corrected clock/ephemeris covariance $\mathbf{P}_w^k$ is given by:

$$\mathbf{P}_w^k = \Lambda - \Lambda\mathbf{G}_w^T \left(\mathbf{G}_w \Lambda \mathbf{G}_w^T + \mathbf{W}^W\right)^{-1} \mathbf{G}_w \Lambda \quad (10)$$

where the measurement-error weighting matrix $\mathbf{W}^w$ is equal to the M x M matrix of RMTSA error variances for each WRS that can see satellite *k*.

4.2 Computer Implementation Procedure

In our computer code, for each updated GPS satellite geometry, the satellite visibility for each WRS is computed and formatted as shown by the matrix $\mathbf{G}_w$ in (8). At this point, the algorithm loops through the grid of user locations that are affected by the WAAS corrections. For each user, $\tilde{\mathbf{G}}_u$ and $\mathbf{G}_u^*$ are computed from $\mathbf{G}_u$ using (2) and (3). $\mathbf{P}^k$ for each satellite in view of this user is then computed using (7) or (10) as required; thus giving the block-diagonal matrix $\mathbf{P}^{SV}$ (6).

At the same time, the parallel computation of the user pseudorange error covariance matrix $\mathbf{\Sigma}_u$ for ionospheric errors is computed using the algorithm in Section 5.0. The effects of RMTSA user ranging errors are computed (see Section 3.0) and summed with $\mathbf{\Sigma}_u$ to get the final user error covariance $\mathbf{P}_v^*$. Finally, the user position covariance $\mathbf{P}_{\hat{x}}$ for this geometry is computed using (5). This process is repeated for each user location, and we store the resulting vertical position error variance, σ_z^2, given by the 3rd diagonal element of $\mathbf{P}_{\hat{x}}$ for each user in a histogram unique to that user location for post-sampling analysis. We also compare the vertical error variance at a given user for each sample geometry to the ILS and RNP tunnel accuracy requirements to compute the overall probability that the resulting vertical position error is within the specified accuracy.

5.0 Ionospheric Grid Error Propagation Model

The ionospheric grid covariance propagation model, run in parallel with the clock/ephemeris model detailed above, directly propagates ionospheric uncertainty from the WRS's to the WMS, which projects the combined corrections onto an artificial "grid" of ionospheric pierce points separated by 5, 10, or 15 degrees of latitude and longitude. This covariance is then propagated to the user depending on the location of his pierce points within the grid structure. Note that this grid concept is similar to that originally proposed by MITRE [5], but it uses weighted least-squares fits to interpolate corrections within the grid rather than simple linear inverse-weighted interpolation.

It is basically assumed by this model that the *vertical* ionospheric delay (i.e. not affected by satellite elevation) observed by a GPS receiver through a given pierce point denoted as $\hat{\mathbf{I}}_p$ can be expressed as the sum of two independent random variables: the *true delay* (denoted as $\mathbf{I}_p$) and the *observation error* (denoted as $\mathbf{\Sigma}_p(\varepsilon)$). This basic relation holds for the WRS's, the WMS, and the user (with the appropriate subscripts). Note that $\mathbf{\Sigma}_p(\varepsilon)$ is elevation-dependent because it represents the RMTSA error terms discussed in Section 3.0.

The propagation of ionosphere error covariance is executed in several distinct steps as follows:

5.1 WRS Covariance

The vector $\mathbf{I}^{\hat{P}}$ contains the measured (via dual-frequency receivers at each WRS) vertical ionospheric delay at each pierce point observed by all WRS's:

$$\mathbf{I}^{\hat{P}} = \begin{bmatrix} \mathbf{I}_{m=1}^{\hat{P}} \\ \mathbf{I}_{m=2}^{\hat{P}} \\ \vdots \\ \mathbf{I}_{m=M}^{\hat{P}} \end{bmatrix} \qquad (11)$$

where $\mathbf{I}_m^{\hat{P}}$ represents the observed delays for each satellite visible to WRS *m*, *m* = 1,..., M_{rms} (the total number of WRS's). The vector $\boldsymbol{\varepsilon}^P$ is a sample of the RMTSA noise distribution. Its covariance, denoted as $\mathbf{\Sigma}^P$, is a diagonal matrix whose variances are computed by summing the RMTSA numbers in Section 3.0 with a constant *interfrequency bias*. This bias represents miscalibrations between GPS satellites and WAAS/user receivers. Based on current bias estimates, we add the square of a conservative bias deviation estimate of σ_{boas} = 0.75 m to each diagonal entry of $\mathbf{\Sigma}^P$. Operational WAAS systems should be able to reduce this by at least 50% [6].

The true ionospheric delay covariance, denoted as $\mathbf{P}^P$, is a function of the geographic separation between the WRS pierce points and the assumed "base" delay variation at a given point over time. The base delay standard deviation σ_b is taken to be 2.8 meters, which is relatively conservative. Based on curve fits to absolute and relative (one station compared to another)

ionospheric delay data appearing in [4,5], the following covariance formulas are used for each entry in $\mathbf{P}^{\mathrm{P}}$ (which will consequently have no zeros in it) [10]:

$$\sigma(d) = \frac{I_{\mathrm{base}}\, I_{\mathrm{mult}}}{OF_{\mathrm{mean}}} \frac{R_{\mathrm{slope}}}{R_{\mathrm{base}}}\, d \qquad (12)$$

where:

d = distance between ref. and observ. PP's (km)
R_{base} = base separation in Klobuchar data = 348 km
R_{slope} = linear slope with dist. in data fit = 0.542
I_{base} = base ionosphere decorr. for (d = 0) = 0.417 m
I_{mult} = ionosphere decorrelation multiplier = 2.0
OF_{mean} = mean obliquity factor in data = 1.763.

If d > D, where D = 1200 km, the effective $\sigma(d)$ is modified by an exponential curve such that $\sigma(d) \le \sigma_b$, where σ_b^2 is the "base" ionospheric variance over time for any given pierce point. This normally varies with geomagnetic position, but we use the conservative value $\sigma_b = I_{\mathrm{mult}}\, \sigma_{\mathrm{norm}}$ = 2.8 m. The resulting equation is:

$$\sigma(d > D) = \sigma(D) + \sigma_{\mathrm{marg}} \left[1 - \exp\left(\frac{-\left[\sigma(d)_{\mathrm{fit}} - \sigma(D)\right]}{\sigma_{\mathrm{marg}}} \right) \right]$$

where $\sigma_{\mathrm{marg}} = \sigma_b - \sigma(D)$, and $\sigma(d)_{\mathrm{fit}}$ is the variance given by (12) for d > D. This variance from one PP to another is converted to a covariance entry [i,j] in matrix $\mathbf{P}^{\mathrm{P}}$ using the Gaussian bivariate relation:

$$\sigma_{i,j}^2 = \sigma_b^2 \sqrt{1 - \left(\sigma_{i,j}(d)/\sigma_b\right)^2} \qquad (13)$$

Summing the covariances $\mathbf{P}^{\mathrm{P}}$ and $\mathbf{\Sigma}^{\mathrm{P}}$ gives $\mathbf{P}^{\hat{\mathrm{P}}}$, the final WRS ionospheric measurement covariance matrix.

5.2 WMS Covariance

The Wide Area Master Station (WMS) is where the pierce-point measurements of the individual WRS's are collected to form $\mathbf{P}^{\hat{\mathrm{P}}}$. The WMS then relates the pierce point delay measurements $\mathbf{I}^{\hat{\mathrm{P}}}$ to those that would exist at the WMS grid points by solving for the optimal choice of mapping matrix **A** using least-squares:

$$\mathbf{A}^{\mathrm{T}} = \mathbf{P}^{\mathrm{G}\hat{\mathrm{P}}} \left[\mathbf{P}^{\hat{\mathrm{P}}} \right]^{-1} \qquad (14)$$

where $\mathbf{P}^{\mathrm{GP}} = \mathbf{P}^{\mathrm{G}\hat{\mathrm{P}}}$ is the "true" covariance (computed using (12,13) between the fixed WMS ionosphere grid points (G) and the set of WRS pierce points (P). From the definition of covariance, we can simplify the application of the mapping matrix to get the final grid point covariance:

$$\mathbf{P}^{\hat{\mathrm{G}}} = \mathbf{A}^{\mathrm{T}} \left[\mathbf{P}^{\mathrm{G}\hat{\mathrm{P}}} \right]^{\mathrm{T}} = \mathbf{P}^{\mathrm{G}\hat{\mathrm{P}}} \left(\mathbf{P}^{\hat{\mathrm{P}}} \right)^{-1} \left[\mathbf{P}^{\mathrm{G}\hat{\mathrm{P}}} \right]^{\mathrm{T}} \qquad (15)$$

where $\mathbf{P}^{\hat{\mathrm{G}}}$ is the resulting covariance of the WMS ionosphere grid points. Note that WRS ionosphere measurement errors are represented in $\mathbf{P}^{\hat{\mathrm{P}}}$ and get propagated into $\mathbf{P}^{\hat{\mathrm{G}}}$ through this process.

5.3 User Covariance

WAAS users (located on a grid of predetermined points covering a wide geographic area) use the transmitted WMS estimates of vertical ionosphere delay at each ionosphere grid point $\mathbf{I}^{\hat{\mathrm{G}}}$ to project ionosphere errors at their pierce points to the satellites they can see. As with WMS propagation, we use least-squares optimal mapping. From the mapping matrix **A** in the previous section, we can find the user-to-grid covariance $\mathbf{P}^{\mathrm{U}\hat{\mathrm{G}}}$:

$$\mathbf{P}^{\mathrm{U}\hat{\mathrm{G}}} = \mathbf{P}^{\mathrm{U}\hat{\mathrm{P}}} \mathbf{A} = \mathbf{P}^{\mathrm{U}\hat{\mathrm{P}}} \mathbf{P}^{\hat{\mathrm{P}}} \left[\mathbf{P}^{\mathrm{G}\hat{\mathrm{P}}} \right]^{\mathrm{T}} \qquad (16)$$

where $\mathbf{P}^{\mathrm{U}\hat{\mathrm{P}}}$ is the user-to-WRS pierce point covariance, computed (as with $\mathbf{P}^{\mathrm{GP}}$) using the spatial decorrelation equations (12,13). The definition of covariance and a second mapping matrix **B** allows us to project the error in the WMS grid to the user's pierce points as follows:

$$\begin{aligned} \mathbf{B}^{\mathrm{T}} &= \mathbf{P}^{\mathrm{U}\hat{\mathrm{G}}} \left[\mathbf{P}^{\hat{\mathrm{G}}} \right]^{-1} \\ \mathbf{P}^{\hat{\mathrm{U}}} &= \mathbf{B}^{\mathrm{T}} \mathbf{P}^{\hat{\mathrm{G}}} \mathbf{B} = \mathbf{P}^{\mathrm{U}\hat{\mathrm{G}}} \left[\mathbf{P}^{\hat{\mathrm{G}}} \right]^{-1} \left(\mathbf{P}^{\mathrm{U}\hat{\mathrm{G}}} \right)^{\mathrm{T}} \end{aligned} \qquad (17)$$

where $\mathbf{P}^{\hat{\mathrm{U}}}$ is the user ionosphere error covariance due to the WAAS fitting algorithm. By our previous assumptions, the basic equation for user ionosphere vertical error covariance $\mathbf{P}_{\varepsilon}^{\mathrm{U}}$ is:

$$\mathbf{P}_{\varepsilon}^{\mathrm{U}} = \mathbf{P}^{\mathrm{U}} - \mathbf{P}^{\hat{\mathrm{U}}} = \mathbf{P}^{\mathrm{U}} - \mathbf{P}^{\mathrm{U}\hat{\mathrm{G}}} \left[\mathbf{P}^{\hat{\mathrm{G}}} \right]^{-1} \left(\mathbf{P}^{\mathrm{U}\hat{\mathrm{G}}} \right)^{\mathrm{T}} \qquad (18)$$

where $\mathbf{P}^{\mathrm{U}}$ is the overall covariance, which can be computed from the underlying decorrelation between the user's pierce points using (12). The last step is to multiply the covariances in the final result, $\mathbf{P}_{\varepsilon}^{\mathrm{U}}$, by *obliquity* factors to convert from vertical to slant pierce point delay. The obliquity factor *OF* is computed by:

$$OF = 1 \Big/ \sin\left(\varepsilon^{'}\right) \approx 1 + 2\left[\frac{96 - \varepsilon\,(\text{deg.})}{90}\right]^3 \qquad (19)$$

where ε is the elevation angle from user to satellite. Each entry of $\mathbf{P}_{\varepsilon}^{U}$ is multiplied by $(OF)^2$ to get the final user slant ionosphere error covariance, $\mathbf{\Sigma}_U$. This final matrix is added to the user RMTSA covariance $\mathbf{P}_{v}^{user}$ to get the "external noise covariance" matrix $\mathbf{P}_{v}^{*}$ in (5). From this, the user position error covariance $\mathbf{P}_{\hat{x}}$ is computed.

5.4 Numerical Difficulties

Because the matrix operations in (14-18) imply the numerical calculation of inverses of large matrices, numerical difficulties can arise even though the C code does not need to explicitly calculate each inverse. The WRS pierce-point covariance $\mathbf{P}^{\hat{P}}$ is usually the most difficult to work with, as it is of size M_P x M_P, where M_P is the total number of pierce points observed by all WRS's. The C code uses double-precision floating-point representation (16 digits), but cases arise where the *condition number* of $\mathbf{P}^{\hat{P}}$, which is the ratio of the largest to the smallest of the *singular values* of $\mathbf{P}^{\hat{P}}$, increases above 10^{12}, meaning that the covariance matrix approaches singularity to double-precision. Since singular matrices are not permitted in the covariance-propagation equations, a numerical breakdown in the calculations may result [12].

The source of near-singularity is the fact that most of the pierce points are located in a relatively small area. Their correlation to each other is thus quite high relative to the underlying ionospheric variation and observation errors (i.e., the diagonal terms). The covariance matrix thus becomes closer to singular (i.e. invalid) as the spatial decorrelation in the off-diagonal terms decreases. We have found that the matrix condition deteriorates as more pierce points are included, since more observations reduce the effective decorrelation. For WAAS architectures (such as the FAA NSTB) where M_p generally exceeds 75, a *parsing* procedure must be employed to ensure adequate numerical conditioning.

Parsing refers to the reduction of the size of $\mathbf{P}^{\hat{P}}$ by merging pierce points that are close together into a single observation (for ionosphere purposes only). $\mathbf{P}^{\hat{P}}$ is computed normally using (12,13) for all pierce points (PP's), then a loop goes through the list of pierce points backward: $j = M_p, \ldots, 1$. If PP j is within a certain threshold distance T_d from another PP i, where $i < j$, PP j is parsed out of $\mathbf{P}^{\hat{P}}$ and PP i is moved to a new location:

$$\mathbf{x}_{\text{new}}^{i} = \frac{a\,\mathbf{x}_{\text{old}}^{i} + b\,\mathbf{x}_{\text{old}}^{j}}{a+b} \qquad (20)$$

where $\mathbf{x}$ is the relevant PP location in *xyz* Earth-fixed coordinates; while a and b are integer weighting factors which count the number of PP's that have been "parsed" into the current PP locations i and j. In addition, the base error variance of the new PP is reduced by:

$$\left(\sigma_{\text{new}}^{i}\right)^2 = \left(\sigma_{\text{old}}^{i}\right)^2 N_{\text{dec}} = \left(\sigma_{\text{old}}^{i}\right)^2 \frac{1}{a+1} \qquad (21)$$

This simply models the noise "averaging" which takes place as more and more WRS's observe a PP in the same general area. The off-diagonal terms are not reduced.

6.0 WAAS User Position Accuracy Results

The covariance propagation method described here has been applied to a variety of existing and planned WAAS networks. Much of the algorithm development was done with variations of the 3-WRS Stanford WAAS (including some with one or two additional WRS's). The RMTSA and ionosphere covariance parameters were derived with results from the Stanford setup in mind. The algorithm is the same (with one change to be discussed below) for the larger FAA WAAS testbed networks, and we have been able to obtain projections for provisional WAAS systems anywhere in the world.

Using MATLAB to plot the results of our C programs, we can present the results as 2-D contours or 3-D surface plots. The program outputs the following data for each user, and the overall results are plotted over a map of the relevant user geography:

- 95% and 99% vertical position error
- 95% and 99% Vertical dilution of precision (DOP)
- Availability = Pr(vertical error σ < ILS requirement)
- Maximum outage duration
- 95% and 99% vertical ionosphere delay error

Recall that for each geometry, the above results were stored in histograms. For the 95% and 99% position error cutoffs, the outer-loop histogram of error variance (over all satellite geometries) is convolved with the Normal distributions implied by the relevant variances [10]. Note that vertical ionosphere delay error (the last bullet) corresponds to "User Ionosphere Vertical Error" (UIVE) in the FAA's terminology [13] and is contained in $\mathbf{P}_{\varepsilon}^{U}$ from (18). "User Differential Ranging Error" (UDRE) for each satellite in view is given by $\mathbf{P}^{SV}$ in (6,7,8) but is not plotted separately at this point.

6.1 Stanford WAAS Results

The current Stanford experimental WAAS network consists of a master station in the Durand building at Stanford University and three reference stations located in San Diego, CA., Arcadia, CA., and Elko, NV. An additional reference station setup exists at Stanford but is used in a "passive user" mode to evaluate the quality of the position solution provided by the three "primary" WRS's [2]. Plans for additional WRS's in Hawaii and Alaska and possible relocations of the three exisiting WRS's have been discussed, motivating us to compute predictions for some of these variations as well.

Figure 2 shows a 2-D contour plot of 95% vertical position accuracy over a user area bounded by 18° to 48° North latitude and 108° to 128° West longitude, divided into one-degree increments. A 10° WMS ionosphere grid is used, extending from 20° to 50° N latitude and 105° to 135° W longitude. The WRS locations are denoted on the map surface by an 'x' in all plots.

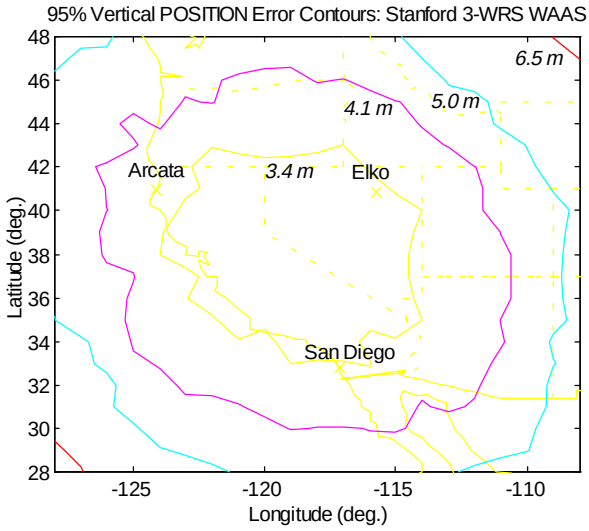

Figure 2: 95% Position Accuracy, Stanford WAAS

The results for 95% user accuracy show that the optimal performance region is relatively flat and encloses an area considerably wider than the area between the three WRS's. Vertical accuracy degrades gracefully as one gets further away from this zone, although the falloff becomes substantial if one gets far enough away, because the WRS observations have little leverage to correct the (probably different set of) satellites a far-away user can see. However, accuracy sufficient to meet the 4.1-meter 95% ILS requirement is provided for users as far away as the Oregon-Washington border and Phoenix, AZ. Note that all users use weighted least-squares to get their position fixes; thus far-away users will optimally deemphasize the satellites for which good WAAS corrections are not available in their position solutions.

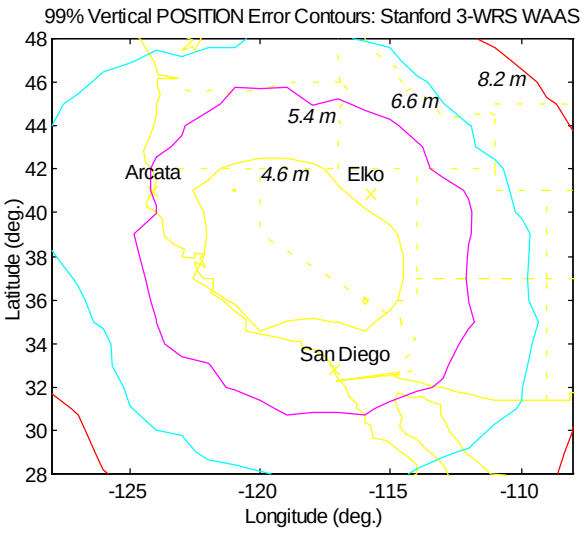

Figure 3: 99% Position Accuracy, Stanford WAAS

Figure 3 gives the 99% vertical position accuracy results for the same system. Note that if the underlying overall distribution were Gaussian, 95% cutoffs would represent 2σ and 99% would result in approximately 3σ, giving an expected multiplication of 1.5. In these results, while the contour shapes are similar, the apparent 99% performance for most user locations is better than 1.5 times the 95% performance shown in Figure 2. The same phenomenon is also observed for the 95% and 99% UIVE contour plots to be discussed later, where in many cases the 99% results are only 10-20% worse. Our results suggest a non-Gaussian or truncated-Gaussian underlying distribution, but given that our method is based on a concantenation of "Normal" conditions only, we are not confident that this is a fair representation of reality. Rather, we believe that a Gaussian distribution is valid out to 95% and that a projection of performance from 2σ to 3σ (i.e. multiplying by 1.5) would be more reasonable than using the 99% histogram results.

Figure 4 gives a 2-D contour plot of 95% UIVE, or user vertical ionosphere delay error. These contours conform very well to the shape of the WRS geographic distribution, and once again, the degradation as one moves away from CA-NV is well-behaved and gradual. The nominal 95% error of under 0.6 meters is difficult to verify using our current database of observed ionospheric errors, but it seems reasonable. We are devising a new method for storing observed ionosphere errors so that a better validation of these predictions can be made. As mentioned above, the 99% UIVE plot gives only slightly higher errors, suggesting that the use of only "normal" conditions may lead to overly optimistic predictions. We instead multiply by 1.5 to represent a 2σ to 3σ projection of Gaussian UIVE distributions, and we are investigating this "tail-probability" behavior in our observed data [2].

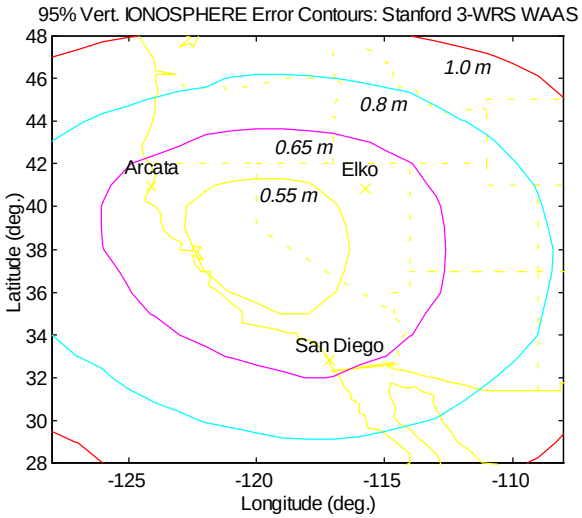

Figure 4: 95% UIVE, Stanford WAAS

6.2 Stanford WAAS Plus Hawaii WRS

Various augmentations to the Stanford WAAS have been proposed. It is now expected that these will be incorporated into the FAA WAAS testbed as it is built. One key augmentation would be the addition of a fourth reference station in Honolulu, Hawaii. It would attempt to both provide Category I accuracy to the Hawaiian Islands and augment our corrections for users in the western Continental U.S (CONUS).

Figure 5 is a plot of 95% vertical position errors for this 4-WRS network over an enlarged user area from 16° to 50° N latitude and 112° to 162° W longitude, divided into 2° increments. A 15-degree ionosphere grid from the Equator to 60° N and from 105° to 165° W was used for the WMS. The considerable distance between Honolulu and the other three WRS's (over 3000 km) is

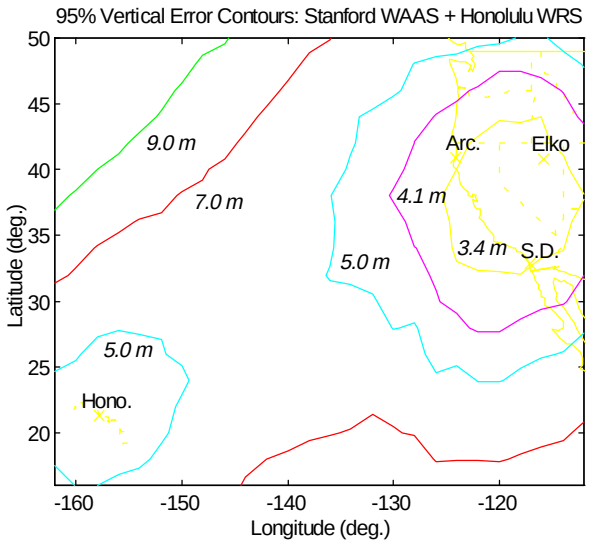

Figure 5: 95% Position Accuracy, Stanford + Hawaii

why the Hawaii WRS only slightly improves CONUS performance (compare to Figure 2). The Hawaii WRS is not quite able to provide ILS Category I accuracy for the area encircling the Hawaiian Islands, but the 95% error is still under 5 m, which would easily meet the relaxed RNP requirement [9]. Significant improvement is attainable by improving the ionosphere calibration (i.e. reducing σ_{bias} in Section 5.1) [6]. Note that the degradation of position accuracy over the Pacific between CONUS and Hawaii is graceful enough to support enroute navigation for air routes between them.

A further motivation for including a WRS in Hawaii is that this WRS would see most satellites before the stations in CONUS, allowing it to begin filtering corrections before the satellites are visible in CONUS. This effect, in which low-elevation rising satellites have larger post-correction pseudorange errors until averaging reduces effective multipath, is not modeled in our "snapshot" covariance algorithms. We are currently measuring this effect in the Stanford WAAS data, and we plan to add it to the RMTSA error model in the future.

6.3 FAA NSTB Testbed Results

In advance of the planned introduction of an operational WAAS in the late 1990's, the FAA plans to build a testbed of about 18 WRS's spread throughout CONUS. This testbed, known as *NSTB*, is designed to experimentally evaluate WAAS user performance and to provide guidance to the development of the operational system [3]. Stanford University is participating in developing and testing WRS and WMS algorithms that may be included in the NSTB. The covariance methods detailed here can also be used to predict NSTB user accuracies over the entire CONUS region.

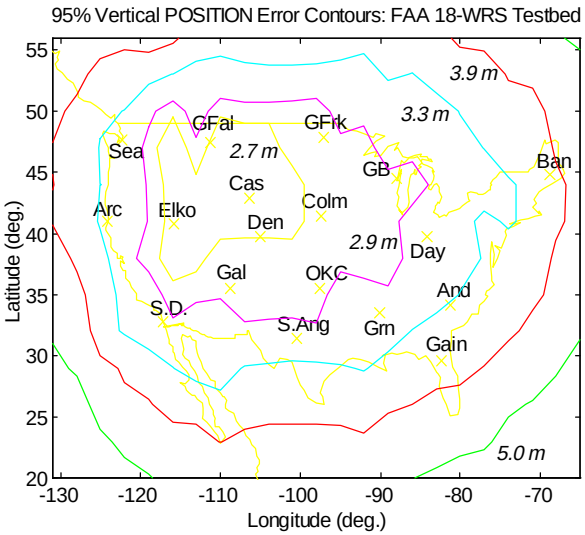

Figure 6: 95% Accuracy, FAA 18-WRS NSTB

Because each of the 18 WRS's in the NSTB sees an average of 8-10 satellites at a time, parsing of the ionosphere covariance matrix $\mathbf{P}^{\hat{P}}$ (see Section 5.4) is necessary. Using a separation threshold T_d = 500 km, the number of rows and columns in $\mathbf{P}^{\hat{P}}$ decreases from an average of 160 to 54 for the 18-WRS NSTB. With this level of parsing, no numerical matrix singularity problems have been observed.

Figure 6 shows a 2-D contour plot of 95% vertical position errors for a 3° user grid from 20° to 56° North latitude and 65° to 131° West longitude. The WMS ionosphere grid goes from the Equator to 75° N and from 50° to 140° W in 15° increments. It is clear that even with conservative ionosphere parameters, 18 WRS's are fully capable of providing ILS Cat. I landing accuracy throughout CONUS. A WAAS 95% "accuracy floor" of about 2.7 m is evident in the Western U.S., where the density of WRS locations is highest. WRS density in the Eastern U.S. is much lower, possibly to serve as a more severe test for landing experiments at the FAA Technical Center in Atlantic City, N.J. Nevertheless, the Eastern U.S. coastline still achieves 95% vertical accuracy of four meters or better.

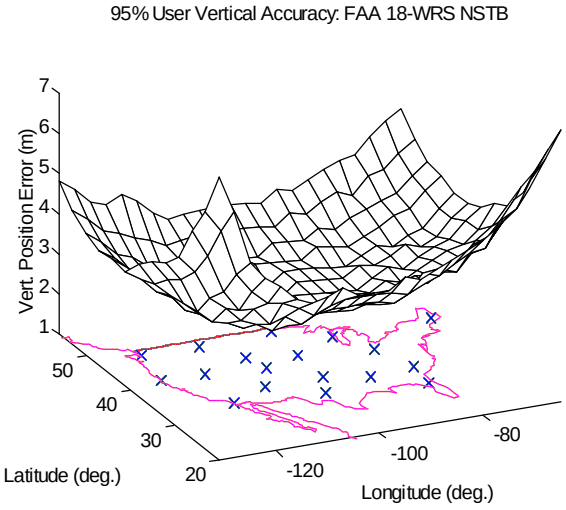

Figure 7: 3-D 95% Accuracy Plot, FAA NSTB

Figure 7 is a 3-D representation of the same position accuracy results. This plot gives a nice overview of the shape of the 95% accuracy surface, or "bowl", over CONUS. As would be expected from the lack of WRS's outside CONUS, the gradient of this surface gets worse near the edges of the user grid. Users off to the southeast or southwest of CONUS have the worst accuracy, but it is still within 7 m. Figure 8 is a similar 3-D plot of the 95% user VDOP surface. It is shown to display the important effect of the added geosynchronous satellites. Note that users in the lowest section of this surface (where 95% VDOP ≈ 1.5) can see *both* the 180° and 55° E SV's, whereas most of the other user locations can only see one of these. Because a basic requirement for WAAS is that each user see at least two geosynchronous SV's (to ensure reception of valid corrections), more of these SV's will be needed for the operational WAAS; thus VDOP should improve further [11].

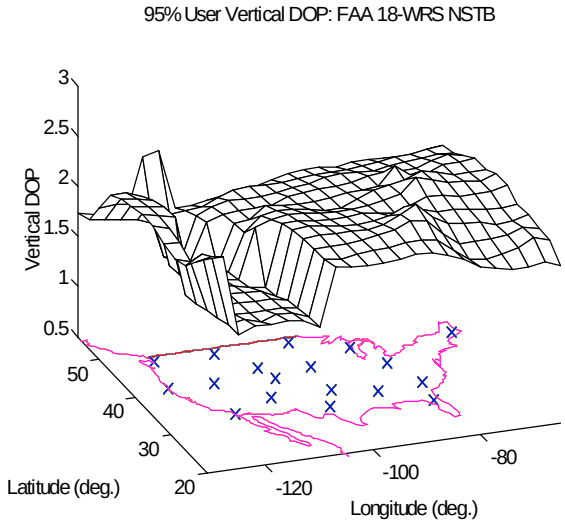

Figure 8: 3-D 95% VDOP Plot, FAA NSTB

Figure 9 is a 2-D contour plot of 95% UIVE for the NSTB. These errors are small even for our conservative ionosphere model parameters. In the center of CONUS, the presence of WRS observations on all sides improves 95% UIVE to below 0.4 m, and all of CONUS is under 0.8 m. This demonstrates how well a nationwide WAAS can fit the underlying ionosphere states under "normal" ionospheric conditions. In solar maximum years, these errors should be no worse than twice that shown here [4].

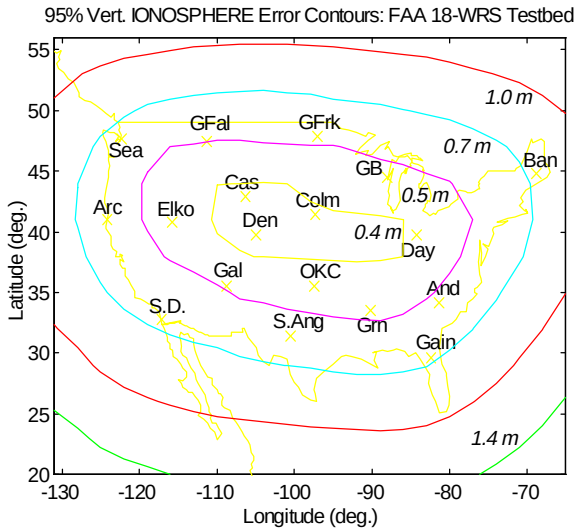

Figure 9: 95% Ionosphere Error, FAA 18-WRS NSTB

The rapid worsening of the user accuracy performance at the edges in Figure 7 motivates a study of adding additional WRS's outside CONUS. Likely sites include Honolulu, HI, Anchorage, AK, Puerto Rico, and Gander, Newfoundland. In addition, it is worth investigating the change in East Coast performance if one of the many WRS in the West is moved to Atlantic City, NJ. Figures 10 and 11 show 95% vertical accuracy and UIVE results for a variant of the NSTB that adds the four WRS's listed above and moves the Casper, WY. WRS to Atlantic City.

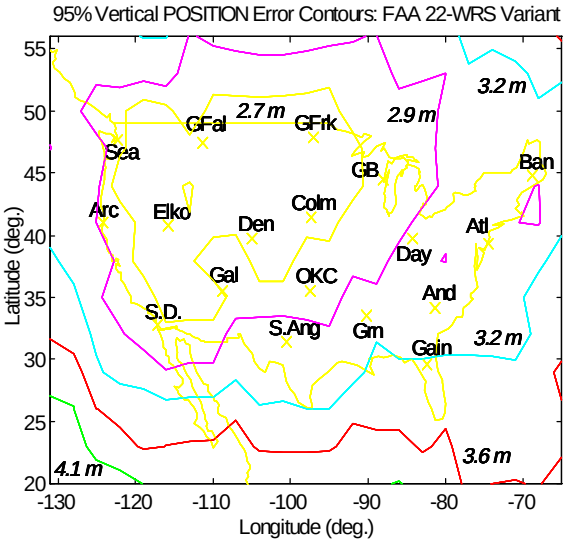

Figure 10: 95% Accuracy, FAA 22-WRS Variant

Figure 10 clearly shows substantial user accuracy improvement compared to the basic NSTB (Figure 7). With these changes, all of CONUS now has 95% vertical error of less than 3.6 m, and the accuracy gradients have lessened along the borders of CONUS. The network is still unbalanced towards the West, but the East Coast has improved markedly. Also note that very little was lost by the removal of the Casper WRS, while much was gained by an addition in Atlantic City. Figure 11 shows that UIVE has improved substantially as well. The variant NSTB provides 95% UIVE under 0.5 m for over 80% of CONUS. Note that the two northern WRS additions are closer to CONUS than the southern ones; thus UIVE improves much more along the northern U.S. border. In contrast, little improvement is gained along the U.S.-Mexico border (a WRS in Mexico would help).

6.4 Summary of Results

The results presented in this section demonstrate that the covariance propagation methods developed in this paper produce useful and sensible predictions of WAAS performance. The Stanford WAAS predictions meet our performance expectations and agree with our limited flight-test data base. The geographic performance degradation is gradual enough to verify that the WAAS

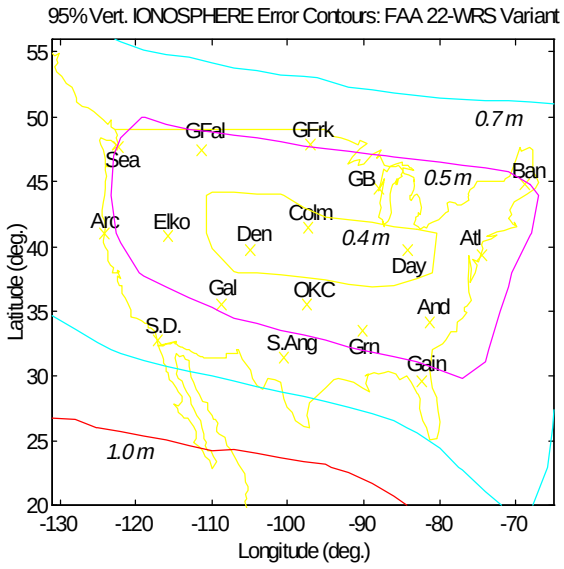

Figure 11: 95% UIVE, FAA 22-WRS Variant

concept can provide truly useful "wide-area" corrections. The addition of a WRS in Hawaii has a limited effect over CONUS since it is far away, but it provides "local-area" accuracy to its own area and helps calibrate the error surface over the region of the Pacific in between.

Predictions for the FAA NSTB suggest that a WRS network of this density is easily able to meet the ILS Category I landing requirement throughout CONUS. A combination of nearby WRS density, geosynchronous satellite visibility, and a bias toward the best-error-fit middle of the WRS region influence a given user's performance in a logical way. The data collected from NSTB starting in 1997 will be the first opportunity to verify these predictions.

Several key points should be raised here regarding the limitations of this methodology for predicting WAAS utility. First, the covariance propagation steps use batch least squares fits to the GPS error surfaces. Given the assumed "white" Gaussian behavior of GPS performance in non-failure cases, a least-squares solution is generally seen to be optimal. However, execution time constraints and the numerical problems mentioned in Section 5.4 make this approach probably infeasible in a real-time WAAS. Instead, numerically easier data fits will be used [1]. Thus, our covariance method represents the assumed *underlying behavior* of GPS errors in a WAAS context. It could therefore be viewed as an algorithmic upper bound on WAAS performance. Instead, we believe that the conservative parameters of our current error models with improve as more data is collected. Furthermore, the process of design-and-test should produce real-time algorithms that are tuned to non-ideal error performance as observed from test results. As a result, we believe that

operational WAAS systems will be able to improve on the predictions contained in this paper.

In addition, the assumption of "normal" WAAS error performance does not allow us to make *integrity* or *continuity* predictions. Indeed, the excellent accuracy predicted for the NSTB in Section 6.3 suggests that adequate integrity is possible but cannot demonstrate it. Monte Carlo sampling has been used to predict integrity performance [8,10], but it would be a major task to do it over a large WAAS user grid. In fact, the relatively high WRS density of the NSTB (and the operational FAA WAAS) can be seen as partially a hedge against worse-than-expected spatial decorrelations. Our confidence in making WAAS integrity predictions will rely critically on further experimental ionosphere results.

7.0 Conclusions and Further Work

Despite the assumptions and limitations of the best GPS/WAAS error models available, we have demonstrated that it is possible to use least-squares covariance propagation to predict the performance that widely-spread-out users will be able to achieve from any candidate WAAS network. This approach has produced reasonable, internally-consistent accuracy predictions for both current prototype WAAS systems and a full-scale NSTB designed to cover all of CONUS. It thus serves as a very useful "end-to-end" computer analysis tool to aid the layout, design, and development of future networks.

Currently, we are using this method to predict WAAS performance while varying the proposed FAA network layouts and some of the key error parameters that go into the covariance model. A key addition is the rising vs. falling satellite error dependence mentioned in Section 6.2. Predictions are also being generated for conceptual WAAS networks covering Western Europe and East Asia. Since we can manually try different configurations and study the changes in accuracy, it is also possible to automate the optimal-network search process, using a combination of accuracy, cost, and (indirect) integrity models to numerically evaluate each alternative. Global search methods such as Simulated Annealing and Genetic Algorithms can be used to converge toward an optimal WAAS architecture for a given user area.

ACKNOWLEDGMENTS

The authors would like to thank the following people for their help with this research: Dr. Changdon Kee, Y.C. Chao, Boris Pervan, Y.J. Tsai, and Dr. Todd Walter. The advice and interest of many others in the Stanford GPS/WAAS research group are always appreciated.

REFERENCES

[1] P. Enge, A.J. Van Dierendonck, "The Wide Area Augmentation System," *Proc. 8th Int'l. Flight Inspection Symposium*, Denver, CO., June 1994.

[2] T. Walter, C. Kee, Y.C. Chao, Y.J. Tsai, *et.al.*, "Flight Trials of the Wide Area Augmentation System (WAAS)," *Proceedings of ION GPS-94*, Salt Lake City, UT., Sept. 21-23, 1994.

[3] R. Loh, "Seamless Aviation: FAA's Wide Area Augmentation System," *GPS World*, Apr. 95, pp. 20-30.

[4] J.A. Klobuchar, P.H. Doherty, and M.B. El-Arini, "Potential Ionospheric Limitations to Wide-Area Differential GPS," *Proceedings of ION GPS-93*, Salt Lake City, UT., Sept. 22-24, 1993, pp. 1245-1254.

[5] M.B. El-Arini and T.C. Wisser, "The FAA Wide Area Differential GPS (WADGPS) Static Ionospheric Experiment," *Proceedings of ION NTM-93*. Anaheim, CA., Jan. 22-24, 1993, pp. 485-496.

[6] Y.C. Chao, Y.J. Tsai, T. Walter, C. Kee, P. Enge, B. Parkinson, "The Ionospheric Model Improvement for the Stanford WAAS Network," *Proceedings of ION NTM-95*, Anaheim, CA., Jan. 18-20, 1995, pp. 531-538.

[7] T. Walter, B. Pervan, P. Enge, J. Herendeen, and P. Levin, "Autonomous Integrity Monitoring and Wide Area DGPS," *Proceedings of ION NTM-94*. San Diego, CA., Jan. 24-26, 1994, pp. 485-496.

[8] T. Walter, P. Enge, F. Van Grass, "Integrity for the Wide Area Augmentation System," *Proceedings of DSNS-95*. Bergen, Norway, April 24-28, 1995, No. 38.

[9] R. J. Kelly, J. M. Davis, "Required Navigation Performance (RNP) for Precision Approach and Landing with GNSS Application ," *Navigation*, Vol. 41, No. 1, Spring 1994, pp. 1-30.

[10] S. Pullen, P. Enge, B. Parkinson, "Simulation-Based Evaluation of WAAS Performance: Risk and Integrity Factors," *Proceedings of ION GPS-94*. Salt Lake City, UT., Sept. 20-23, 1994, pp. 975-983.

[11] W. Phlong, B. Elrod, "Availability Characteristics of GPS and Augmentation Alternatives," *Navigation*, Vol. 40, No. 4, Winter 1993-94, pp. 409-428.

[12] W.H. Press, et.al., *Numerical Recipes in C: The Art of Scientific Computing, 2nd Ed.* Cambridge, England: Cambridge University Press, 1992.

[13] M.B. El-Arini, C.J. Hegarty, J.P. Fernow, and J.A. Klobuchar, "Development of an Error Budget for a GPS Wide-Area Augmentation System (WAAS)," *Proceed. of ION NTM-94*, San Diego, CA., Jan. 24-26, 1994, pp. 927-936.

[14] Y.J. Tsai, "Snapshot WMS Algorithms for Ephemeris and Clock Estimation," Stanford University, Unpublished Manuscript, Feb. 13, 1995.